Surface Salinity Retrieved from SMOS Measurements over the Global Ocean: Imprecisions Due to Sea Surface Roughness and Temperature Uncertainties

Jacqueline Boutin, Philippe Waldteufel, Nicolas Martin, Gérard Caudal, Emmanuel P. Dinnat

Surface Salinity Retrieved from SMOS Measurements over the Global Ocean: Imprecisions Due to Sea Surface Roughness and Temperature Uncertainties

JACQUELINE BOUTIN

Laboratoire d'Océanographie Dynamique et de Climatologie/Institut Pierre Simon Laplace, UMR UPMC/CNRS/IRD, Paris, France

PHILIPPE WALDTEUFEL

Service d'Aéronomie/Institut Pierre Simon Laplace, Verrières-le-Buisson, France

NICOLAS MARTIN

Laboratoire d'Océanographie Dynamique et de Climatologie/Institut Pierre Simon Laplace, UMR UPMC/CNRS/IRD, Paris, France

GÉRARD CAUDAL

Centre d'etude des Environnements Terrestre et Planétaires/Institut Pierre Simon Laplace, IUT de Vélizy, Vélizy, France

EMMANUEL DINNAT*

Laboratoire d'Océanographie Dynamique et de Climatologie/Institut Pierre Simon Laplace, UMR UPMC/CNRS/IRD, Paris, France

(Manuscript received 5 August 2003, in final form 25 January 2004)

ABSTRACT

The Soil Moisture and Ocean Salinity (SMOS) mission recently led by the European Space Agency (ESA) intends to monitor soil moisture and sea surface salinity (SSS). Since the sensitivity of radiometric L-band signal to SSS is weak, measuring SSS with an acceptable accuracy is challenging: it requires both a very stable instrument and very precise corrections of other geophysical signals than the SSS affecting the L-band signal. Concentration is on the sea surface roughness and temperature (SST) effects and the extent to which they need to be corrected to optimize both SSS precision and retrieval complexity. In addition to uncertainties regarding SST and wind speed (W), realistic noise on the SMOS brightness temperatures (Tb's) are considered and possible consequences of Tb biases are examined.

In most oceanic regions, random noise in W, SST, and Tb should not hamper the SMOS SSS retrieval within the Global Ocean Data Assimilation Experiment (GODAE) requirements (a precision better than 0.1 pss over 200 km $\times$ 200 km and 10 days). However, minimizing systematic bias errors over the time scale at which the SSS products will be averaged is critical: the GODAE requirement will not be met if Tb's or W is biased in warm waters (25°C) by 0.07 K and 0.3 m s^{-1}, respectively, and in cold waters (5°C) by 0.03 K and 0.15 m s^{-1}, respectively, or if no a priori information on W is available. In order to minimize errors coming from the W natural variability, it is essential to use high-temporal-resolution wind data. The use of the first Stokes parameter instead of bipolarized Tb degrades the SSS precision by less than 10% in most regions, showing that Faraday rotation should not hamper SMOS SSS retrieval.

1. Introduction

Studies conducted in the late 1970s and early 1980s showed that it is theoretically possible to measure sea surface salinity (SSS) using L-band radiometry (Swift and McIntosh 1983). However, since the ground resolution of measured pixels is proportional to the radiometer wavelength and inversely proportional to the antenna aperture diameter, a real aperture antenna several meters wide is necessary to monitor SSS from satellite with a surface resolution suitable for oceanographic studies (e.g., on the order of 10–50 km to resolve mesoscale eddies or of 100–200 km for constraining ocean circulation models). This hindered the development of L-band satellite missions during the previous decades. Recently, new satellite projects for measuring SSS that

* Current affiliation: European Space Agency, Noordwijk, Netherlands.

Corresponding author address: Dr. Jacqueline Boutin, LODYC/IPSL, UMR UPMC/CNRS/IRD 7617, 4, place Jussieu, 75252 Paris Cedex 05, France.
E-mail: jb@lodyc.jussieu.fr

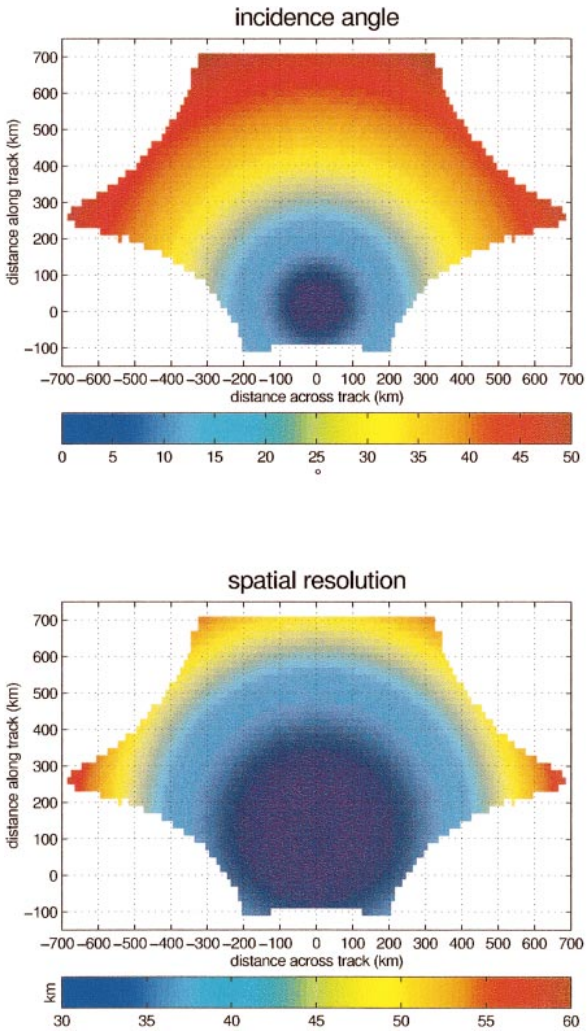

FIG. 1. Distribution of (top) incidence angles and (bottom) pixel spatial resolution in SMOS FOV.

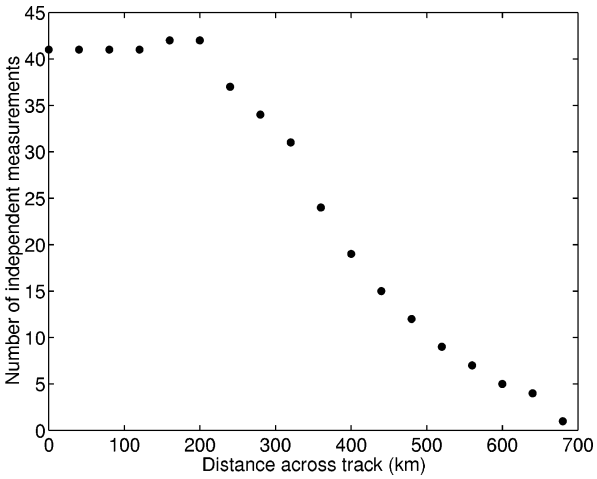

FIG. 2. Number of independent (Tv, Th) measurements in pixels resampled at 40 km across track, from the center to the edge of the swath; note that the number of independent measurements is twice the one plotted in the figure (dual polarization).

take advantage of technical improvements have emerged. In that context, the Soil Moisture and Ocean Salinity (SMOS) mission, supported by the European Space Agency (ESA) (see http://www.esa.int/esaLP/smos.html for more details), uses a new two-dimensional interferometric design for L-band passive remote sensing, allowing a spatial resolution at ground level of several tens of kilometers with three coplanar antenna arms approximately 4 m long (Kerr et al. 2001; Silvestrin et al. 2001) that are more easily deployable from space than a real aperture antenna to be achieved.

The precision of individual brightness temperature (Tb) measurements achievable with such a technology will be a few a kelvins. This is very poor compared to the typical sensitivity of Tb to SSS: at nadir it varies from 0.7 K pss^{-1} for a 30°C SST to 0.2 K pss^{-1} for a 0°C SST, whereas the SSS encountered over the open ocean only varies from 32 to 38 pss ["pss" is for practical salinity scale (Lewis 1980), now widely used for oceanic salinity measurements; in the following it is equivalent to parts per thousand in mass of seawater]. Nevertheless, the SMOS two-dimensional field of view provides the opportunity of combining Tb measured over the same pixel at several incidence angles [see Figs. 1 and 2, which were derived from instrument field-of-view simulations (Waldteufel et al. 2003)]. Waldteufel et al. (2003) showed that such a combination allows the SSS random uncertainty to decrease to less than 0.7 pss in 40 km × 40 km pixels, in warm waters at the center of the swath. On the edges of the swath, this figure is larger because the number of independent measurements drops off due to alias elimination.

The present study is an extension of the Waldteufel et al. (2003) study in which SSS errors were estimated theoretically for equatorial pixels at a constant salinity of 35 pss from unbiased Tb. It is aimed at specifying the precision and accuracy of Tb, *W,* and SST suitable for SSS retrieval.

The method employed to estimate the SSS errors is described in section 2. In section 3, we study SSS errors obtained after a single satellite pass in 40 km × 40 km resolution pixels caused by noise and biases in Tb, *W,* and SST. In section 4, we examine SSS errors over the global ocean induced by random noise in SMOS Tb measurements, *W,* and SST. We concentrate on SSS precision at scales of 200 km × 200 km and 10 days, which are relevant for a large number of oceanographic studies. At these space and time scales the Global Ocean Data Assimilation Experiment (GODAE) group recommended SSS products having an optimized precision of 0.1 pss, the minimum requirement being a precision better than 1 pss. Results are discussed and summarized in sections 5 and 6.

2. Methods

A complete description of the SMOS interferometer can be found in Kerr et al. (2001). We consider here the optimal configuration foreseen for SMOS satisfying the science requirements and compatible for a minisatellite (Waldteufel et al. 2003): an antenna plane tilted by about 32°, a satellite altitude of 755 km, a spacing ratio between receiving elements of about 0.88, and 21 receiving elements per arm.

SMOS is equipped with a Y-shaped antenna that permits reconstruction of 2D fields of brightness temperatures. The domain of interferometric baselines is star-shaped. Given the 2D corresponding field of view (FOV) for reconstructed brightness temperature fields, a single area over the earth will be seen at various incidence angles (Fig. 1, top) because of the overlapping of successive FOV as the spacecraft moves ahead. The SSS retrieval will make use of a set of radiometer measurements with various spatial resolutions (Fig. 1, bottom) performed at various incidence angles.

The Stokes parameters in the antenna frame are linear combinations of the Stokes parameters in the sea surface reference frame (Waldteufel and Caudal 2002). In the following, the upwelling third and fourth Stokes parameters (U and V) will be neglected, as they are supposed to be very small, and brightness temperatures measured on the two orthogonal antenna ports will be referred to as Tx and Ty, respectively. Brightness temperatures in horizontal and vertical polarization in the sea surface reference frame will be referred as Th and Tv, respectively.

We investigate the impact on retrieved SSS of uncertainties in ocean surface parameters foreseen to be used in the inversion scheme and in the Stokes parameters themselves because they are expected to be main contributors to the SSS error derived from Tb measured in L band (Lagerloef et al. 1995; Yueh et al. 2001).

The sensitivity of Tb to SSS, SST, and W is derived from the two-scale emissivity model described in Dinnat et al. (2002), which is based on the Yueh (1997) model. In the version used in this study, the influence of SSS and SST on the seawater permittivity is described by the Klein and Swift (1977) parametrization; the wave spectrum is chosen to be the Durden and Vesecki (1985) spectrum multiplied by a factor of 2 as proposed by Yueh (1997). In this configuration, the sensitivity of Tb to the wind speed is twice the one considered in Waldteufel et al. (2003). We choose it because recent comparisons of the Tb sensitivity to the wind speed predicted by the model with the one observed during the 2000 and 2001 Wind and Salinity Experiment (WISE) and Eurostarrs campaign have shown reasonable agreement at low to moderate W values (Camps et al. 2002; Etcheto et al. 2003, 2004). We do not include any parameterization for foam effect since the effect of foam on Tb at L band is poorly known and is expected to be smaller than at higher frequencies (Reul and Chapron 2002).

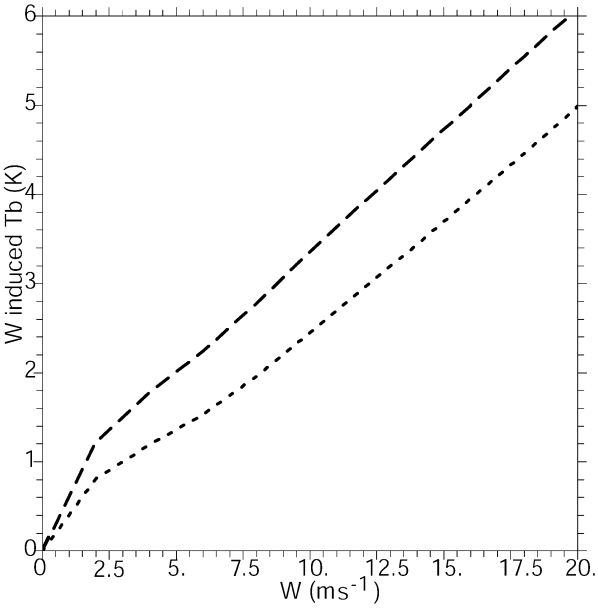

FIG. 3. Brightness temperature (Tb) signal induced by wind speed at nadir (short dashes) and in horizontal polarization at 30° incidence angle (long dashes). Note that the effect in vertical polarization at 30° incidence angle is similar to the effect at nadir. SSS and SST were taken as 36 pss and 25°C, respectively; modifying these values does not affect strongly the dependence of Tb upon W (Dinnat et al. 2003a).

Therefore, the sensitivity of Tb to W for large W values might be underestimated.

An example of the wind speed–induced contribution to Tb is shown in Fig. 3 as a function of wind speed. Above 2 m s^{-1}, Tb was linearly interpolated between model values computed at 2 m s^{-1} intervals. Below 2 m s^{-1}, Tb was linearly interpolated between the model value at 2 m s^{-1} and the value at 0 m s^{-1} deduced from the Fresnel reflexion coefficients for a flat sea. Then Tb versus W is strongly nonlinear at low wind speed. Such a nonlinear behavior has been observed in situ at S band by Blume et al. (1977) and at L band during the WISE experiment (Etcheto et al. 2003, 2004). Nevertheless, the behavior of the model at low wind speed must be taken with great caution since the wave spectrum is not well defined at low wind speeds.

The SSS retrieval error caused by random noise in W, in SST, and in the radiometric measurements (i.e., radiometric sensitivity) is estimated by inverting the Jacobian of the set of Tb with respect to SSS, W, and SST using the generalized inverse method of Jackson (1972). This method gives very similar results to the Marquardt (1963) method that was used in Waldteufel et al. (2003). We have neglected errors on the incidence angles, ϑ. Errors of the Proteus platform pointing angle are specified to be less than 0.05° at 3σ. When taking into account SMOS arms oscillations, present indications are that ϑ errors should be less than 0.03° (at 1σ) and that the statistical distribution of the errors in all ϑ measured

in the FOV should be close to random. Under these assumptions, adding ϑ error in our simulations would increase the resulting SSS error by less than 0.4%.

The retrieved SSS biases caused by biases in initial values specified in the inversion were investigated using Monte Carlo simulations of noisy and possibly biased Tb's, *W,* and SST. For each considered bias, 2000 SSS retrievals were performed in a given 40 km × 40 km pixel, applying the Jackson (1972) method to the noisy and biased Tb, *W,* and SST; the SSS retrieval bias in each pixel was derived from the average of the 2000 retrieved SSSs. Note that only a constant Tb bias over the FOV has been considered.

3. SSS uncertainties in 40 km × 40 km pixels

In this section we neglect the Faraday rotation. Then the SSS is supposed to be retrieved from the set of Tx and Ty measured at different incidence angles in the same pixel.

We study the uncertainties during only one satellite pass (a combination of several satellite passes will be studied in section 4). We consider a 1.5-s elementary integration time for each measurement made at both polarizations; this is equivalent to a 20-km spatial spacing between successive measurements along track; the spacing of independent pixels across track is variable according to the location of the pixel in the FOV. In addition, the spatial resolution of the pixels depends on their location in the FOV. In order to combine measurements made at several locations, we first resample them at a fixed resolution across track (e.g., 10 km), better than the smallest measurement's resolution; then, in order to get errors at a typical resolution of SMOS measurements 40 km × 40 km, we estimate the SSS errors at every 40 km across track by combining the 10-km oversampled SSS errors. In the following, the SSS error and bias will be referred to as σ_{sss} and B_{sss}, respectively. In order to consider the true number of independent measurements, the original resolution of the SMOS measurements is taken into account in these calculations, as detailed in the appendix [Eq. (A1)].

a. Effect of noise

We take into account noise in Tb related to the SMOS instrument characteristics (ranging from 1.6 to 3.9 K for a 1.5-s elementary integration time on each polarization) (Waldteufel et al. 2003). We also take into account noise in the auxiliary parameters used in the inversion: a *W* rms error of 2 m s^{-1} and an SST rms error of 1°C are taken as typical of uncertainties derived from remotely sensed measurements or from operational meteorological model estimates. (Note that noise in the ancillary parameters would have no impact on σ_{sss} if Tb's were perfectly known because in that case SSS would be overdetermined.) The computation was made with initial values of 35 pss and 7 m s^{-1} for SSS and *W,* respectively. Other initial SSS and *W* values give similar patterns and are considered in section 4.

Figure 4a shows σ_{sss}. Since the number of independent Tb measurements is maximum in the center of the swath and since the sensitivity of Tb to SSS is maximum at high SST, σ_{sss} increases with decreasing SST (at the center of the swath, it varies from 0.7 pss at 30°C to 1.5 pss at 0°C), and it increases with increasing distance of the pixel from the center of the swath (at 20°C the error varies from 0.8 pss at the center of the swath to 1.1 pss at 400 km and to 2.3 pss at 650 km). In order to examine the contribution of Tb noise to σ_{sss}, Fig. 4b shows the SSS error (relative to σ_{sss}) given an error in Tb only. At the edge of the swath, more than 90% of σ_{sss} is due to noise in Tb as the number of independent Tb measurements decreases from swath center to swath edge. At the center of the swath, about 50% of σ_{sss} comes from noise in Tb. Figure 4c shows the SSS error due to errors in Tb and in *W* normalized to σ_{sss}. The contribution of SST noise to σ_{sss} is always less than 5%, and at the center of the swath about 50% of σ_{sss} is due to *W* a priori uncertainty (Figs. 4b,c).

b. Effect of biases

In addition to adding noise in initial values as in section 3a, we add biases in Tb's, SST, or *W,* named in the following input biases. We tested the addition of various input biases: the resulting SSS biases vary linearly with them. Hence, only retrieved SSS biases obtained for 1-K Tb biases, for 1°C SST bias, or for 1 m s^{-1} *W* bias are reported in Fig. 5 as SSS biases because other input biases can be linearly derived from Fig. 5 values. The largest biases occur at low SST as the sensitivity of Tb to SSS decreases with SST. The SSS biases due to Tb biases are significant: −1.4 pss K^{-1} at 25°C and −2.5 pss K^{-1} at 10°C; this indicates that an SSS accuracy of 0.1 pss requires a Tb bias less than 0.07 K at 25°C and less than 0.04 K at 10°C. The combination of measurements made at various incidence angles does not permit correction for biases. Wind speed biases also introduce significant SSS biases [0.4 pss $(m\ s^{-1})^{-1}$ at 25°C and 0.6 pss $(m\ s^{-1})^{-1}$ at 10°C]. On the other hand, biases in SST do not strongly bias SSS except at low SST (0.2 pss $°C^{-1}$ at 10°C).

SSS biases do not strongly vary with the pixel location across track, as can be seen in Fig. 5. Only the computations made with initial values of 35 pss and 7 m s^{-1} for SSS and *W,* respectively, are shown; computations conducted with other initial values are very similar.

It must be noticed that since the across-track variations of the retrieved SSS biases are very small, SSS retrieved from input parameters biased homogeneously over a given region and time would be biased by an almost constant value. So, input biases homogeneous in a GODAE box would lead to biases on retrieved SSS similar to the ones we derived in individual pixels. Of

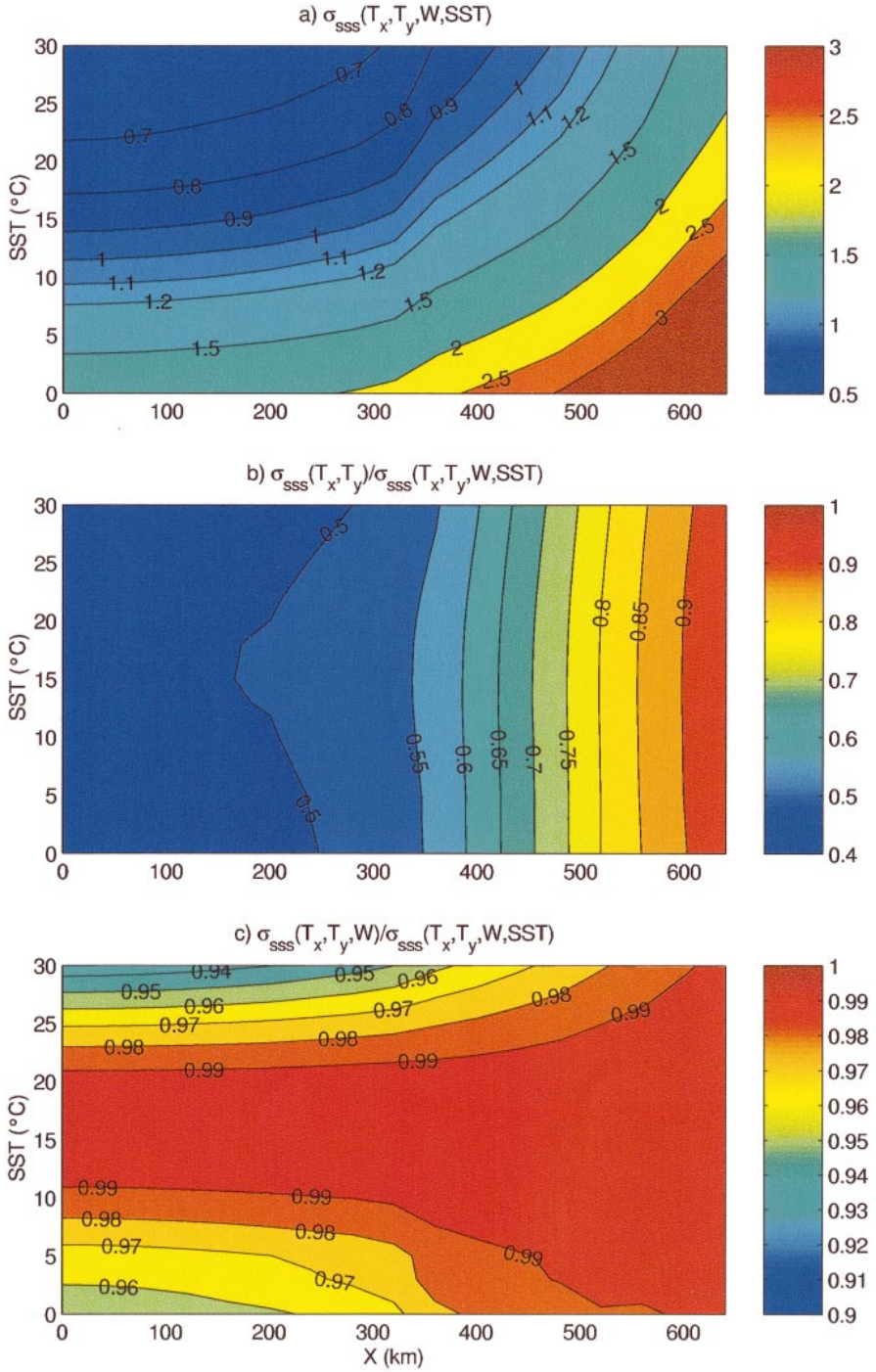

FIG. 4. (a) SSS uncertainties (pss) across track from the center of the swath to the swath edge, in pixels at 40 km × 40 km resolution, given noise in Tb, *W*, and SST. (b) Proportion of SSS error due to noise in Tb. (c) Proportion of SSS error due to noise in Tb and in wind speed.

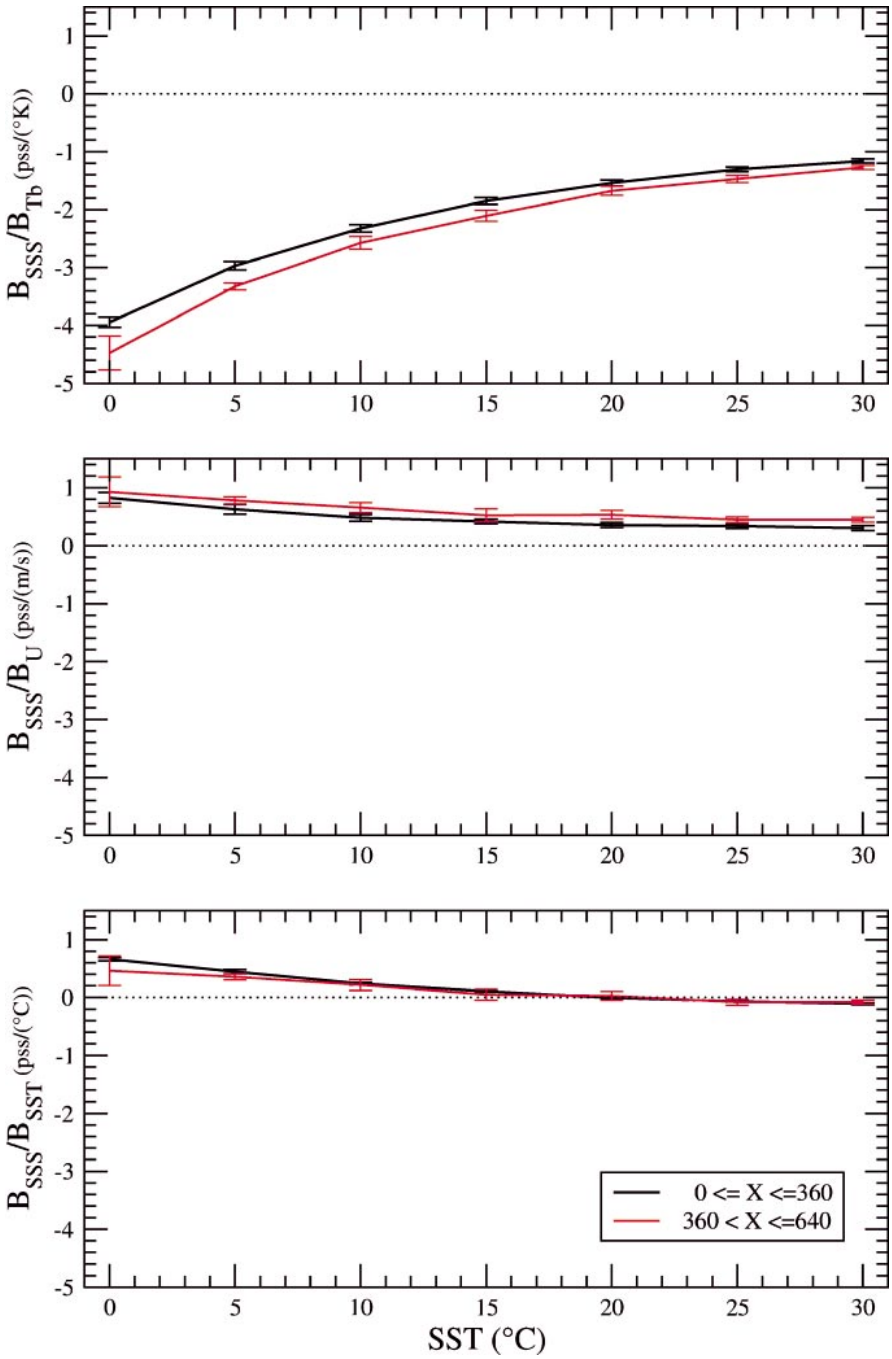

FIG. 5. SSS biases (pss) caused by biases in input values: (a) 1-K bias in Tb's, (b) 1 m s^{-1} bias in *W*, and (c) 1°C bias in SST. Mean of SSS biases at the center of the swath (±400 km from the center) (black) and at the swath edge (360–600 km from the center) (red) are reported together with the std dev of the biases derived in 40-km pixels.

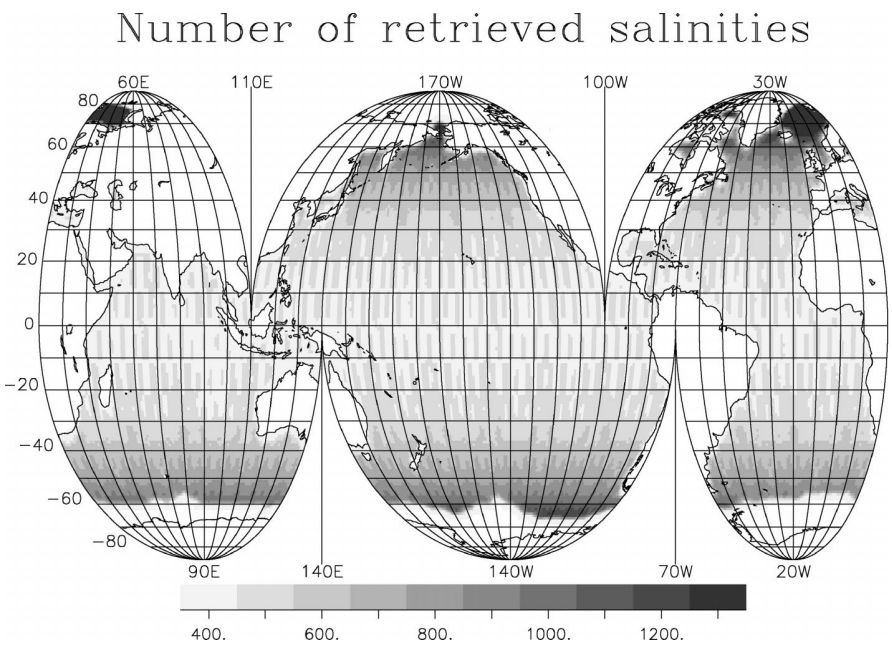

FIG. 6. Number of salinities retrieved in 200 km × 200 km over 10 days.

course, this would not be the case if input biases were variable over 10 days or 200 km × 200 km.

4. Uncertainties in SSS averaged over 200 km × 200 km and 10 days

We now consider uncertainties in SSS at larger time and space scales. We perform error simulations over the global ocean, taking into account a simulated SMOS orbit. Several scenarios were envisaged: 1) the use of multiangular dual-polarized Tb measurements and instantaneous noisy SST without any a priori knowledge of the wind speed; 2) same as scenario 1 but with instantaneous noisy wind speed; 3) the use of average (instead of instantaneous) wind speed; and 4) the use of the first Stokes parameter (I = Tx + Ty) (instead of dual-polarized measurements), which is intended to study to what extent a correction of dual-polarized Tb for the Faraday rotation effect is relevant. Lastly, since the Faraday rotation is expected to be at maximum in the evening while it can most probably be corrected with a good precision during the morning orbit (LeVine and Abraham 2002; Skou 2003), we study a scenario closer to the most realistic physical conditions that will be referred to in the following as ''most realistic scenario'' and in which we use noisy ancillary parameters (wind speed and SST) and dual-polarized measurements for the morning orbit and the first Stokes parameter for the evening orbit.

We first derive the SSS uncertainties at each satellite pass in 200 km × 200 km resolution pixels and then average the variance of these uncertainties over 10 days to estimate the ''mean error'' as described in the appendix. Then a large number of independent measurements are combined: each salinity is retrieved from several tens of independent Tb's [about 40 pairs of (Tv, Th) close to the swath center, see Fig. 2] and 400–1000 retrieved salinities are averaged (see Fig. 6).

These simulations were conducted during 10 days for the period 21–31 July 1999. In order to consider a realistic space and time variability of W, we built daily 40-km-resolution wind speed fields by interpolating along the SMOS track instantaneous 25-km-resolution wind speeds derived from QuikSCAT measurements provided by the Jet Propulsion Laboratory (JPL) (Dunbar et al. 2001). Since the temporal variability of SST is small, we use a field of SST averaged over 2 weeks and 1° derived from the Reynolds analysis (Reynolds and Smith 1994). The initial SSS field is the World Ocean Atlas climatology (Antonov et al. 1998) for July. A summary of these fields is presented in Fig. 7.

a. Unknown wind speed

We take the same random noises in SST and Tb as in section 3. An error of 20 m s^{-1} is put in W, which is equivalent to considering it as unknown.

Figure 8 (top) shows the resulting SSS error over the globe. The error in the estimated SSS is above 0.1 pss at high latitudes and even in some locations in the Tropics. Large uncertainties close to the continents are due to the small number of satellite measurements. The smallest uncertainties are observed in regions of low wind speed for which the sensitivity of Tb to W is higher than at moderate wind speeds (see Fig. 3), allowing a better estimate of W from SMOS measurements. For

SST and SSS values encountered in the open ocean, the error in W retrieved from one SMOS pass in 40 km × 40 km pixels at nadir is ~2 m s^{-1} at low wind speed (~3 m s^{-1}), whereas it is ~3.4 m s^{-1} at moderate wind speed (~8 m s^{-1}). The larger uncertainties at high latitudes are explained by a smaller sensitivity of Tb to SSS at cold SST values.

The uncertainty increase with latitude in the Southern (winter) Hemisphere is primarily due to an SST decrease. In the Northern (summer) Hemisphere, SST is warmer so that the uncertainties, at equivalent latitude, are, in most cases, lower than in the Southern Hemisphere. The large uncertainties in the Hudson Bay are due to very low SSS for which the Tb sensitivity to SST increases so that the impact of SST error on SSS error increases.

b. Instantaneous wind speed

We take the same input random noises in SST and Tb as in section 3. Values of W, derived either from scatterometry or from meteorological analyses, are usually of worse quality at low and high wind speeds; therefore, we assume a random noise in W that depends on its intensity: 2 m s^{-1} below 3 m s^{-1}, 1.5 m s^{-1} between 3 and 15 m s^{-1}, and 10% of W above 15 m s^{-1}.

Figure 8 (bottom) shows the resulting SSS error over the globe. Over the global ocean the error in SSS averaged over 10 days is below 0.1 pss everywhere except close to the ice edges and close to the continents. Between 30°S and 30°N, the error is below 0.05 pss. Again, the almost constant error in this region comes from compensation between a decrease of SST with latitude and a better satellite coverage at higher latitudes; the uncertainties are maxima in the winter hemisphere.

With respect to the previous scenario (scenario a, unknown wind speed, see section 4a and Table 1) the SSS is retrieved with a precision improved by a factor varying from 1.5 in regions of low wind speeds to 2.5 in regions of moderate to strong wind speeds; on average over the global ocean the improvement is a factor close to 2.

c. SSS retrieval uncertainties when neglecting the high-frequency variability of wind speed

It would be much simpler in the retrieval scheme to use only one wind speed average over 10 days than instantaneous wind speeds. We study here the consequences of not taking into account the high-frequency variability of the wind speed. We simulate the 10-day SSS error in the case SSS is retrieved using only a wind speed average over 10 days. In that case the instantaneous wind speed uncertainty $\langle W_{\text{error}} \rangle$ increases, because of the natural variability of the wind speed. We estimate it as

$$\langle W_{\text{error}} \rangle = \sqrt{(s_W^2 + \sigma_W^2/N)}, \quad (1)$$

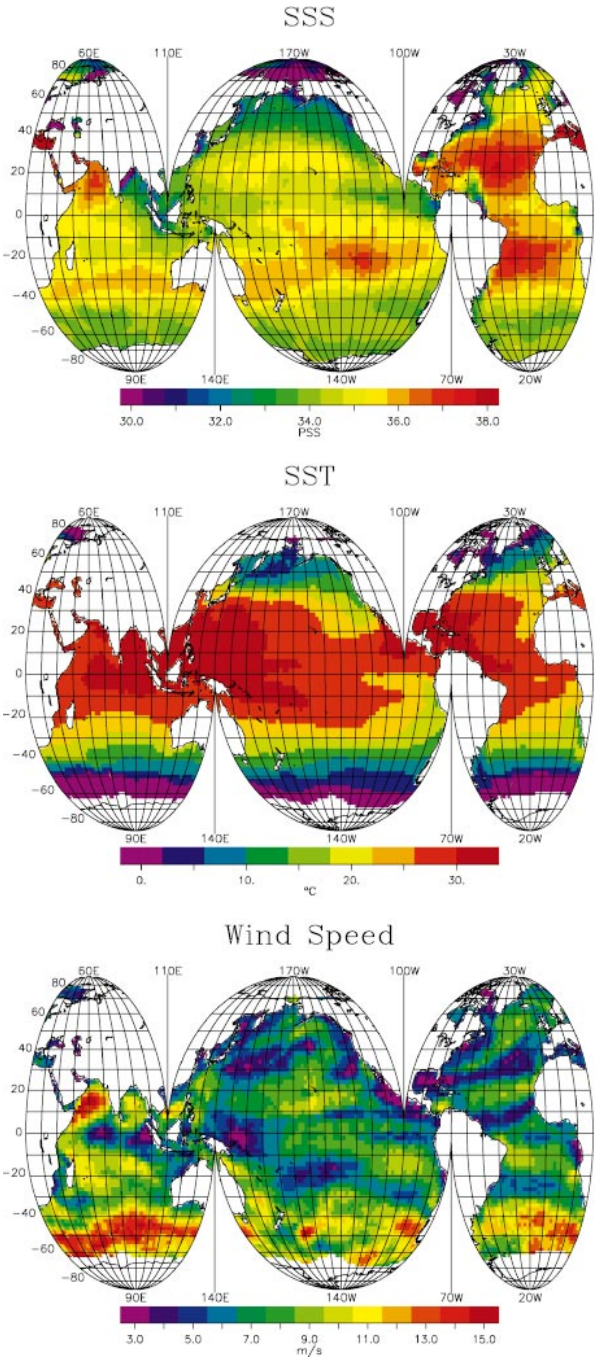

FIG. 7. Global maps of (top) SSS for Jul, (middle) SST from 15 to 29 Jul 1999, and (bottom) 10-day average wind speed from 21 to 31 Jul 1999, illustrating the environmental conditions at the time of the error simulation.

where s_W is the natural standard deviation of the wind speed over 10 days and 200 km × 200 km, σ_W is the wind speed uncertainty defined in section 4b for individual wind speed measurements, and N is the number of measurements used to deduce the wind speed aver-

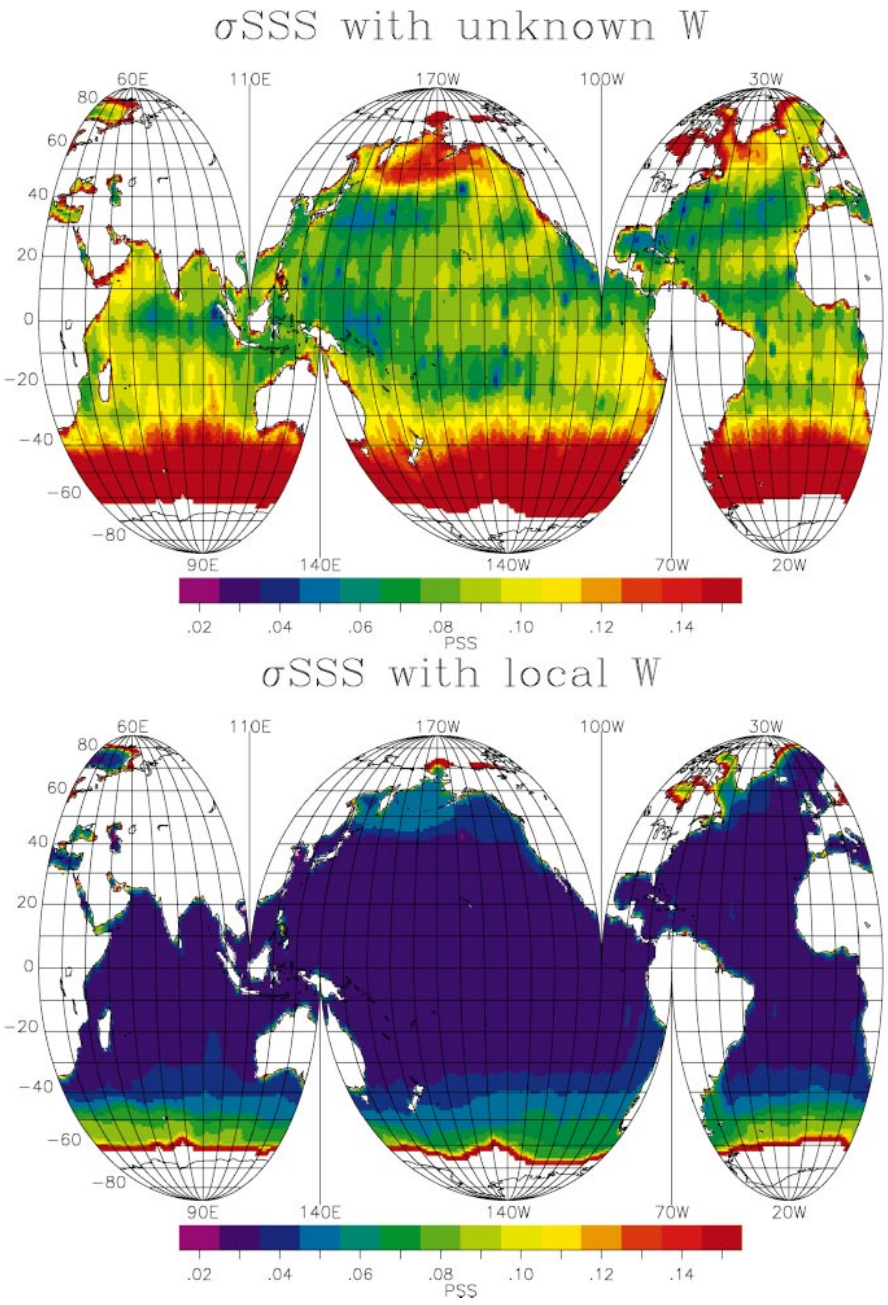

FIG. 8. Uncertainties in SSS averaged in 200 km × 200 km boxes and over 10 days. Use of dual-polarized Tb and (top) unknown wind speed and (bottom) instantaneous wind speed.

age. In (1) we assume that the natural wind speed variability is Gaussian distributed; this is a rather raw approximation that has been taken to ease the computations and that has been shown to be acceptable for many applications (see, e.g., Boutin and Etcheto 1991). We deduced s_W from the standard deviation of QuikSCAT 25-km wind speeds in 2° rasters (see Fig. 9) (we take the wind speed variability in 2° × 2° representative of the wind variability in 200 km × 200 km, and N is equal to the number of SMOS pixels falling in 200 km × 200 km pixels during 10 days).

When only a 10-day-averaged wind speed is used in the inversion as the available a priori information on W, SSS uncertainties are increased in regions of variable wind speeds and become well above 0.1 pss at latitudes higher than 40° in the winter hemisphere (Fig. 10, top). In the Tropics, the increase of errors with respect to scenario b (instantaneous wind speed) is less than 20%

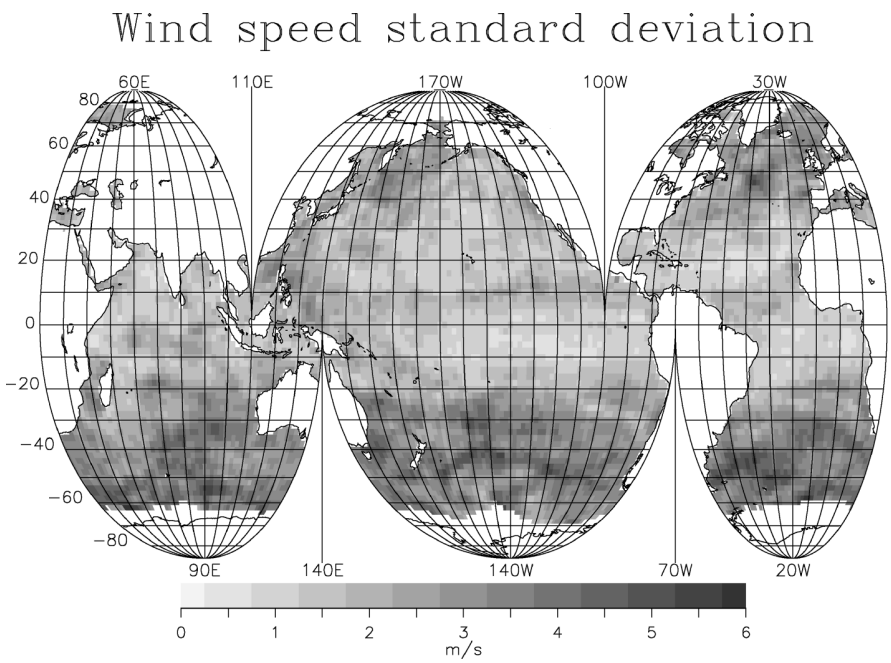

FIG. 9. Std dev of the wind speed in 2° × 2° pixels over 10 days.

(Fig. 10 bottom) because instantaneous W errors are on the same order as W natural variability. In regions with small W variability, the use of an average W may even slightly improve the retrieval; this occurs in case the natural variability of the wind, s_W, is well below the noise of instantaneous W measurements, σ_W. Nevertheless, this slight improvement has to be taken with caution since it has been obtained under the assumption that the wind speed natural variability is Gaussian, which is only true as a first approximation.

On the other hand, outside the Tropics, the high variability of the wind speed leads to an increase of the SSS error of more than a factor of 1.5 when using a W average instead of instantaneous W. Given that about half of the error in SSS retrieved from instantaneous wind speed measurements comes from the wind speed error (see Figs. 4b,c), a factor of 1.5 in Fig. 10 (bottom) indicates that the error due to wind speed has been multiplied by a factor of 2. This simulation was conducted over 10 days during summer in the Northern Hemisphere; the uncertainties in the Northern Hemisphere would be much higher in winter because SST would be colder and W stronger and more variable.

d. Use of the first Stokes parameter

Another source of uncertainty is the Faraday rotation that modifies the polarization ratio of the sea surface emissivity when the signal propagates through the ionosphere. In the presence of Faraday rotation effect, the first Stokes parameter I is conserved. In order to minimize the Faraday rotation effect, one should either correct it (Skou 2003) or use I instead of Tx and Ty, thereby losing half of the independent measurements. In the following, we study the SSS uncertainties determined as in scenario b but using only measurements of I instead of Tx and Ty. Figure 11 shows the 10-day SSS uncertainties obtained from I with respect to the error obtained using two polarizations. If the sensitivity of I to SSS were on the same order as the one of Tv and Th to SSS, this error ratio would be about $\sqrt{2}$ times that obtained using Tv and Th because the number of independent measurements is divided by 2. In fact, the error ratio is less than $\sqrt{2}$ because I is about twice as sensitive to SSS as Tv and Th separately.

Using Tx and Ty or using I is roughly equivalent at high latitudes in cold SST regions. On the other hand, differences up to 10% occur in low-salinity/high-temperature regions (e.g., close to Indonesia and in the eastern tropical Pacific) and at swath edges, because the sensitivity of the first and second Stokes parameters to SSS and SST vary differently depending on SSS, SST, and incidence angles.

Nevertheless, in most regions, the absence of any assumption on the Faraday rotation (i.e., the use of the first Stokes parameter) leads to an uncertainty increased by less than 10% with respect to the use of dual-polarization Tb.

e. "Most realistic" scenario

The Faraday rotation is expected to be maximum in the evening (LeVine and Abraham 2002) and is probably rectifiable with a good precision during the morning orbit. Therefore, we study a "most realistic" scenario in which

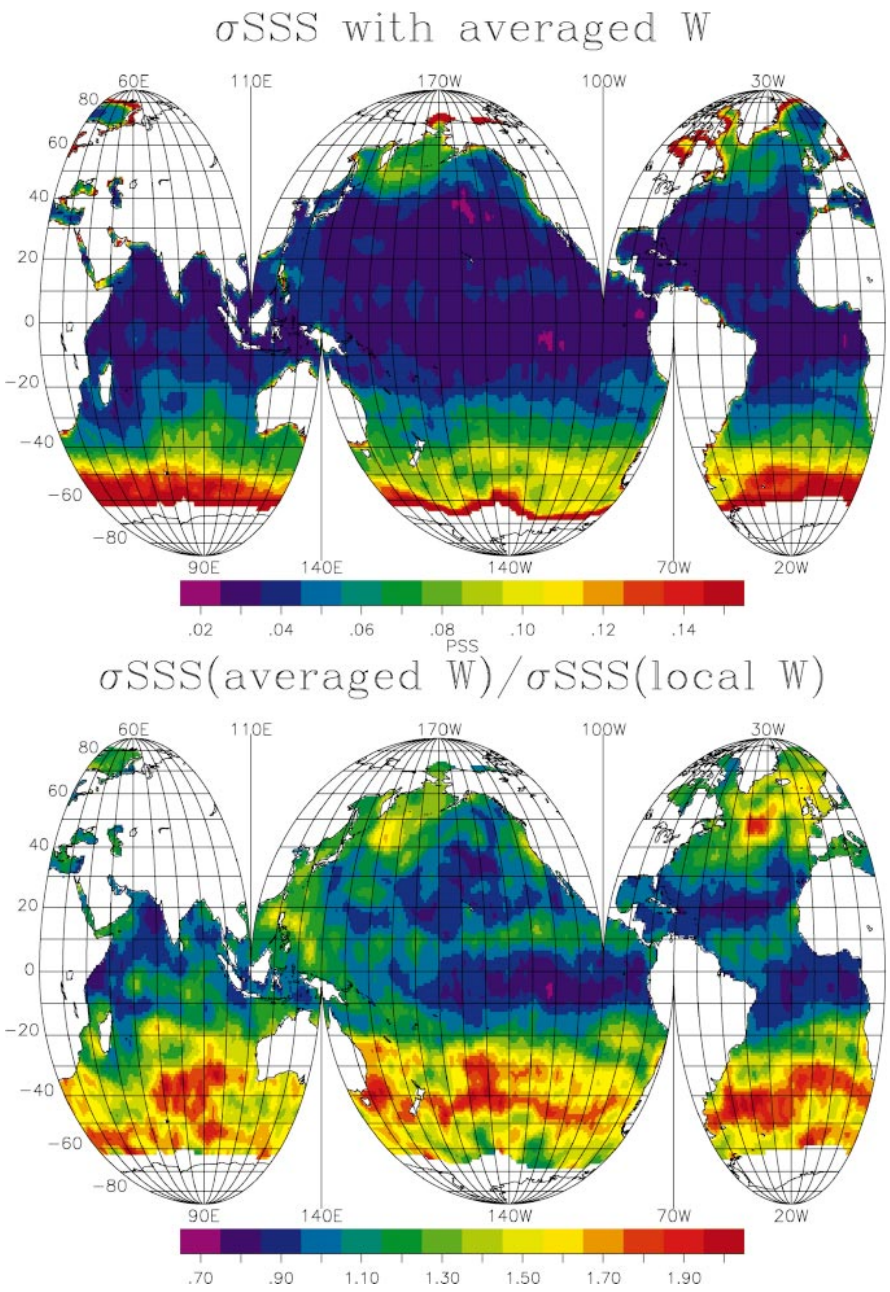

FIG. 10. Use of dual-polarized Tb and 10-day-averaged wind speed. (top) Uncertainties in SSS averaged in 200 km × 200 km boxes and over 10 days. Same color scale as previous figures. (bottom) Ratios of the values shown in top of Fig. 8 to uncertainties obtained with an instantaneous wind speed (see section 4b and Fig. 6).

we use dual-polarized measurements during the morning orbit and first Stokes parameter during the evening orbit. Figure 12 depicts the resulting SSS uncertainties, assuming the instantaneous wind speed data are available, for 10 days in January (top) and July (bottom).

As the use of I almost does not degrade the SSS in cold regions, the SSS error remains comparable to scenario b at high latitudes, and so less than 0.1 pss almost everywhere. With respect to scenario b, it is slightly increased at low latitudes. In January, errors north of 40°N reach 0.08 pss in large areas due to SST decrease with respect to July.

Table 1 summarizes the SSS uncertainties obtained for SSS averaged in 200 km × 200 km pixels over 10 days with the five tested scenarios, both over the global ocean and in the Tropics between 30°N and 30°S. We

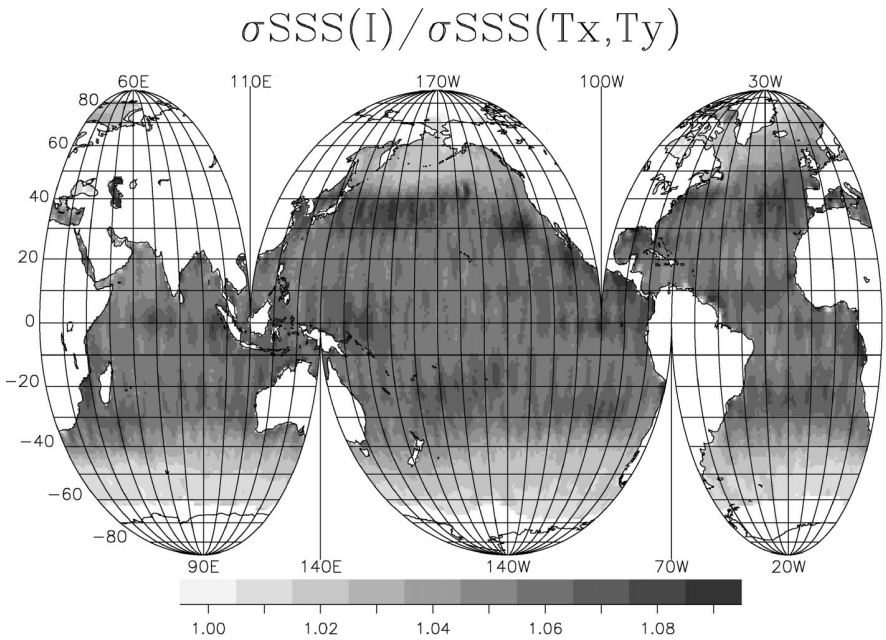

FIG. 11. Ratio between uncertainties in SSS retrieved from the first Stokes parameter and uncertainties in SSS retrieved from Tx and Ty.

do not consider pixels with SSS uncertainties larger than 0.3 pss close to the continents. Whatever the scenario, the mean error in the tropical band is about 30% lower than the one computed over the global ocean. The main differences between these scenarios come from differences in *W* quality, whereas the use of I does not strongly impact the SSS precision.

5. Discussion

This section discusses the consistency of previous estimates for retrieval uncertainties in the general frame of SMOS measurement errors.

a. Calibration accuracy requirements

Requirements in terms of calibration accuracy are critical: SSS bias less than 0.1 pss over 200 km × 200 km and 10 days requires Tb bias over the same space and time scales to be less than 0.04 K at 10°C (less than 0.07 K at 25°C). This is stringent when compared to SMOS capabilities. The SMOS payload is made of two parts: the interferometer that provides relative visibility functions and three noise injection radiometers (NIRs) that provide normalization of the interferogram. The former is expected to undergo many instrument errors; however, they will be monitored by frequent onboard calibration. The resulting residual errors are expected to be mostly random and to average over the FOV down to about 0.05 K (Anterrieu et al. 2003); the latter will be very thoroughly characterized before launch; accounting for corrections based on the monitoring of physical temperatures and power supply on board, the stability of the NIR response curve over 1 month is expected to better than 0.05 K.

In addition to Tb biases, biases on auxiliary parameters will possibly occur. The critical auxiliary parameter is the wind speed: bias in *W* smaller than 0.3 m s^{-1} at 20°C and 0.2 m s^{-1} at 10°C is necessary to achieve an SSS bias less than 0.1 pss, provided that it is the only biased parameter. As shown by Waldteufel et al. (2003), the effect of a *W* bias depends on the a priori error stipulated in *W* (taken as 2 m s^{-1} in our study) so that increasing the a priori *W* error could reduce the SSS bias, but this would be a small improvement since it would lead to less precise SSS that would not meet GODAE requirements in cold waters (see Fig. 8). SST is less critical because it is expected to be biased by less than 1°C and should not hamper unbiased SSS retrieval (within 0.1 pss) in warm waters (above 15°C); it becomes a critical parameter in cold waters.

In the present study, biases in Tb, *W,* and SST were not considered in 10-day simulations because 1) global constant biases are expected to be mostly corrected by vicarious calibration, and 2) time and space distribution of Tb biases are likely to be caused by imperfections in elementary antennas, solar effects, attitude errors, etc., which are difficult to anticipate, especially in the absence of any flying SMOS-like instrument. However, the requirements inferred from the 40-km pixel study are applicable to GODAE scales assuming that Tb, *W,* or SST is homogeneously biased at spatial and temporal GODAE scales, otherwise, in case Tb biases are inhomogeneously distributed in the FOV, part of the SSS

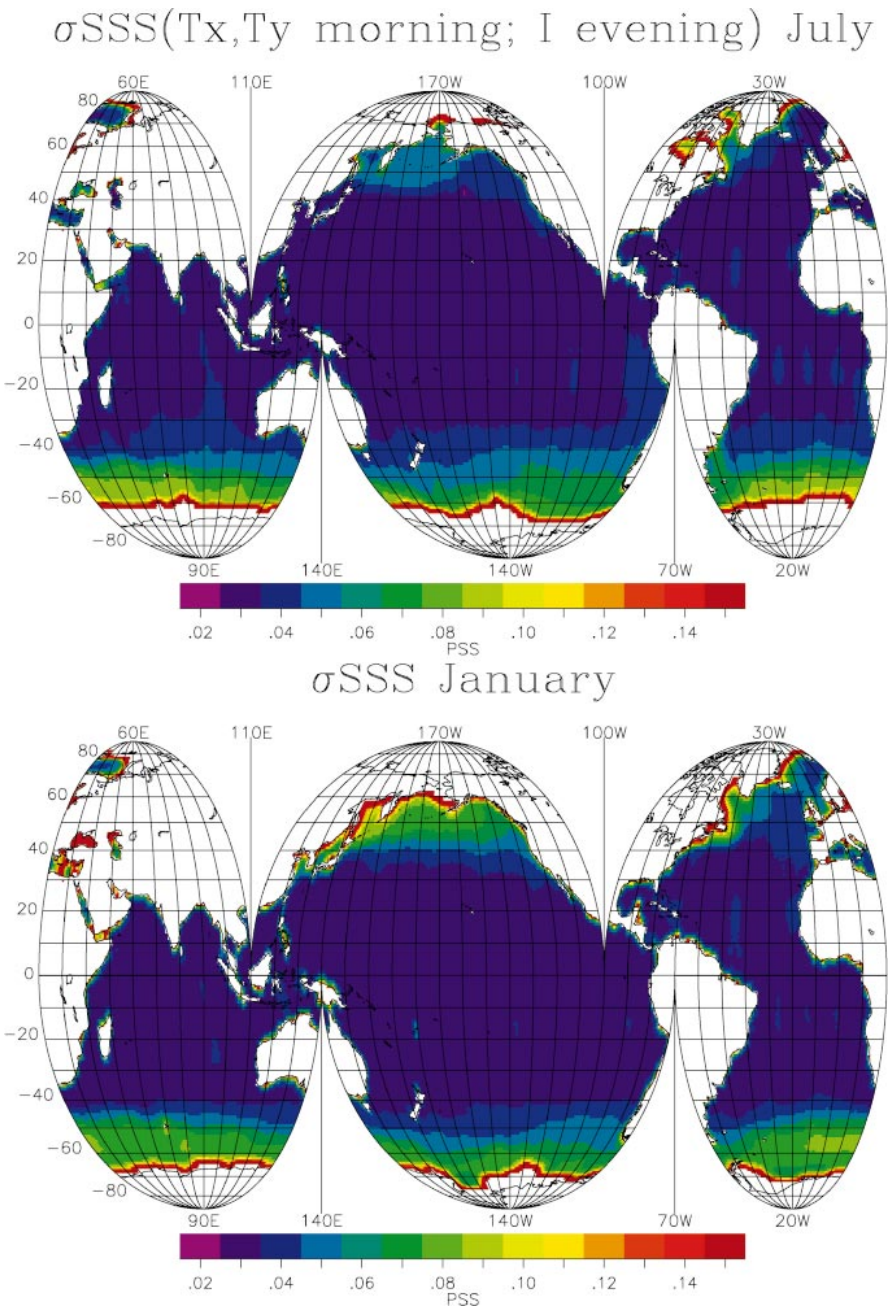

FIG. 12. SSS uncertainties obtained when using dual-polarized Tb during morning orbit, I during evening orbit, and instantaneous wind speed measurements for (top) Jan and (bottom) Jul.

biases in 40 km × 40 km pixels could compensate each other when combined in GODAE pixels, thus decreasing the resulting SSS bias.

b. Precision and auxiliary parameter resolution requirements

Apart from the biases issue, random noise in Tb, wind speed, and SST are shown to induce uncertainties in 10-day, 200 km × 200 km averaged SSS less than 0.1 pss everywhere in the open ocean, provided that instantaneous wind speed estimates are used in the SSS inversion. SST imprecision within 1°C is not a major issue. The Faraday rotation should not be a major issue either since using the (Faraday rotation free) first Stokes parameter induces a loss of precision in most cases less than 10%. On the other hand, considering the wind speed as an unknown in the SSS retrieval scheme for

TABLE 1. Mean ($\langle\sigma$SSS$\rangle$) and std dev std(σSSS) of the SSS uncertainties according to various scenarios (pss).

	Global ocean		30°N–30°S	
Scenario	$\langle\sigma$SSS$\rangle$	Std(σSSS)	$\langle\sigma$SSS$\rangle$	Std(σSSS)
(a) Unknown *W**	0.116	0.050	0.089	0.027
(b) Instantaneous *W**	0.055	0.038	0.042	0.023
(c) *W* averaged over 200 km × 200 km–10 days*	0.069	0.044	0.046	0.025
(d) Instantaneous *W*; use of I	0.057	0.038	0.044	0.023
(e) Realistic scenario	0.056	0.038	0.043	0.023

* Inversions of Tx and Ty measured during morning and evening orbits.

SMOS prevents meeting the GODAE requirements at high latitudes and increases the SSS error by a factor of 2, on average, over the global ocean. This is because at moderate wind speed SMOS measurements allow retrieval of wind speed with a poor precision (typically 3.5 m s^{-1}) that is worse than the one usually achieved with scatterometer measurements and models.

The use of 10-day, 200 km × 200 km average wind speeds is also not sufficient at high latitudes. Nevertheless, in regions of low wind speed variability, this choice degrades the SSS retrieval uncertainty by less than a factor of 1.2. An intermediate choice could be the use of successive instantaneous wind speed averages over 200 km × 200 km. The natural daily variability of *W* in 200 km × 200 km, taken as the standard deviation of daily QuikSCAT wind speeds over 2°, is typically between 0.5 and 1.5 m s^{-1}. Therefore, taking the same reasoning as in section 4c and according to Eq. (1), a 200-km wind speed estimate instead of 40-km estimates would increase the error in the wind speed used in the retrieval by less than 0.03 m s^{-1}, which is negligible. Therefore, the use of high-spatial-resolution wind speed is not critical, whereas high-temporal-resolution wind speed is necessary.

The *W* noise (1.5–2 m s^{-1}) we consider in this study is slightly larger than *W* precision expected for *W* issued from scatterometer measurements or meteorological models. Although it is of the order of magnitude of the rms difference between scatterometer and in situ (buoy or ship) wind speed measurements (Bentamy et al. 1999; Bourassa et al. 1997), recently Freilich and Dunbar (1999) and Quilfen et al. (2001), using a more elaborate method to separate uncertainties in the in situ and in the scatterometer measurements, established that most of the differences come from noise and errors in the in situ measurements, so that noise on scatterometer wind speeds is probably less than 1 m s^{-1}. Concerning meteorological model wind speeds, H. Hersbach (2002, personal communication) estimates a precision of 1.1 m s^{-1} for European Centre for Medium-Range Weather Forecasts (ECMWF) first-guess wind speeds at 40-km resolution, using comparisons of ECMWF *W* with buoy and scatterometer wind speeds. The latter does not take into account spatial correlations between the ECMWF *W* errors that are likely to occur since the final minimization of the cost function is done at 120-km resolution, but it is foreseen that the resolution of meteorological wind fields will improve in the next years.

c. Emissivity model imperfections

As discussed previously in section 5b, the *W* noise we consider appears to be slightly pessimistic. Nevertheless, these results have been obtained assuming that the emissivity model is correct and that roughness effect can be parameterized in terms of wind speed only. In fact, nonwind effects such as sea surface state and surface currents are expected to modify the roughness; part of them will be not systematic in every 40-km pixel over 200 km × 200 km and 10 days and are implicitly taken into account in our *W* noise. On the other hand, these nonwind effects also affect scatterometer measurements: Kelly et al. (2001) and Quilfen et al. (2001) have shown that scatterometer wind speeds may suffer from regional and seasonal biases coming from nonwind effects that on some occasions reach 1 m s^{-1}. In case of L band, Dinnat et al. (2003b) have estimated that the difference on I obtained for a not fully developed sea with respect to a fully developed sea reaches a maximum of 0.2 K at nadir, corresponding to a maximum impact of 0.2 pss on SSS. This is not negligible, but if scatterometer wind speeds are going to be used in the retrieval, errors in L-band modeling and in scatterometer modeling associated with these effects might partly compensate each other.

Even in the absence of nonwind effects, the dependence of Tb with wind speed must also be known with accuracy better than 0.03 K. The results presented in this study use an emissivity model that has to be validated and improved. Although Tb's obtained with this model are inside the error bars of the measurements conducted during several campaigns like WISE 2000, WISE 2001 (Camps et al. 2001, 2002), and the European Salinity, Temperature and Roughness Remote Scanner campaign (EuroSTARRS) (Etcheto et al. 2003, 2004), these experiments were local and it is difficult to extend their results to the global ocean. On the other hand, it is important to study the sources of errors even with imperfect models, to get insights into the critical parameters that will be necessary to take into account in the calibration/validation plans.

We have not taken into account the wind direction,

assuming dependence of Tb with it to be negligible. According to recent scatterometer validations, wind direction is usually retrieved with an error within $\pm 20°$ (Bourassa et al. 1997; Dickinson et al. 2001). We performed sensitivity tests taking into account wind direction with such a bias; biases in SSS up to 0.1 pss appear on some part of the swath. However, when several parts of the swath are averaged together, these biases compensate one another so that the resulting SSS bias over 10 days is negligible.

Although the emissivity model considered here is probably imperfect, the conclusions should remain valid even with a slightly different Tb–W dependence. It is unlikely that Tb–W dependence is very different since it is compatible with existing measurements. Future studies are nevertheless needed to define the best model to be used in the SSS retrieval, both locally with prelaunch aircraft campaigns and at global scale after SMOS launch.

6. Conclusions

The expected precisions on SMOS radiometric measurements and on auxiliary parameters to be used in the SSS retrieval should not hamper meeting the GODAE requirements. On the other hand, requirements in terms of calibration accuracy are very stringent. This stresses the need for a sustained effort to handle the problem of calibration accuracy of both radiometric measurements and auxiliary parameters and the need for an external vicarious calibration based on in situ measurements: the definition of the need in terms of methods and of in situ measurements has to be addressed in order that useful SSS measurements can be performed with SMOS. Yet, the global calibration of the direct emissivity model after launch should help to adjust the model including possible systematic biases of the ancillary parameters.

Acknowledgments. We are indebted to Y. Kerr for providing simulations of SMOS orbits and to J. Etcheto for constructive remarks. We thank H. Hersbach and Erik Andersson for useful discussions about ECMWF wind fields. This work was supported by CNES TAOB Contract 50T207 and ESA Contract 14273/00/NL/DC.

APPENDIX

SSS Uncertainties Computations: Noise on Tb, *W*, and SST

At a given abscissa x_j across the FOV, the SSS is assumed to be retrieved from the measurements obtained for various incidence angles α during successive FOVs. The associated SSS rms error σ_j is derived by the Jackson (1972) method. The computation is repeated for N_j values of x_j abscissa evenly spaced by δx; δx is chosen to be smaller than any pixel size R: for example, $\delta x = 10$ km, whereas R lies in the 30–50-km range.

The SSS estimate at 200 km $\times$ 200 km resolution during one satellite pass, $\langle \mathrm{SSS} \rangle$, is assumed to be derived from a weighted average of all independent SSSj estimates falling in this large box,

$$\langle \mathrm{SSS} \rangle = \left[\sum_{j=1}^{Nj} \mathrm{SSS}_j/(R_j\sigma_j^2) \Big/ \sum_{j=1}^{Nj} 1/(R_j\sigma_j^2) \right]^{1/2},$$

where R_j values are averages of R values for every incidence angle entering in the retrieval. The weight is the inverse of the variance of the estimate multiplied by the pixel size. This is intended to put less weight onto pixels at the edge of the swath associated with large uncertainties. Doing that, we neglect the natural variability of the SSS between typically 40 and 200 km because it is expected to be smaller than the SSS error at 40-km resolution (cf. Fig. 4a).

We then compute a quadratic average rms error $\langle \sigma_j \rangle$ over a range Δx across the FOV. When considering the GODAE requirements, $\Delta x = 200$ km and $N_j = 20$. The average is done in the same way as the SSS average: it is weighted by the inverse of the product of pixel size R_j by the local variance σ_j^2 itself:

$$\langle \sigma_j \rangle = \left[\sum_{j=1}^{Nj} 1/R_j \Big/ \sum_{j=1}^{Nj} 1/(R_j\sigma_j^2) \right]^{1/2}. \quad \text{(A1)}$$

Considering a $\Delta x \Delta y = 200$ km $\times$ 200 km area, the averaging process illustrated by Eq. (A1) is extended to the N_y retrievals obtained along track, resulting in $\langle \sigma_{xy} \rangle$;

$$\langle \sigma_{xy} \rangle = \left[\sum_{k=1}^{Ny} \sum_{j=1}^{Nj} 1/Rjk \Big/ \sum_{k=1}^{Ny} \sum_{j=1}^{Nj} 1/(R_{jk}\sigma_{jk}^2) \right]^{1/2}, \quad \text{(A2)}$$

where $N_y = \Delta y/\delta y$, and δy is the along-track spacing corresponding to successive datasets. Note that these datasets are fully independent. In the SMOS scenario, N_y is of the order of 10. The corresponding rms error σ_{path} for a single orbit is then $\langle \sigma_{xy} \rangle$ divided by the square root of the (N_xN_y) number of independent SSS estimates:

$$\sigma_{\mathrm{path}} = \langle \sigma_{\mathrm{xy}} \rangle / \sqrt{N_xN_y}. \quad \text{(A3)}$$

Contrary to the assumptions made for computing the SSS average over 200 km $\times$ 200 km during one satellite pass, the SSS average made over 10 days is assumed to be made over varying salinities, because the natural temporal SSS variability is assumed to be of the same order or even larger than σ_{path}. Thence, the error decreases temporally as $1/\sqrt{(N_{\mathrm{path}})}$, N_{path} being the number of satellite passes during 10 days. The error over 10 days, $\sigma_{10\mathrm{days}}$, is then derived as the quadratic average of σ_{path} computed at each satellite pass over 200 km $\times$ 200 km boxes:

$$\sigma_{10\mathrm{days}} = \sqrt{1 \Big/ \sum_{i=1}^{N\mathrm{path}} 1/\sigma_{\mathrm{path}\_i}^2}. \quad \text{(A4)}$$

REFERENCES

Anterrieu, E., P. Waldteufel, and G. Caudal, 2003: About the effects of instrument errors in interferometric radiometry. *Radio Sci.,* **38,** 8044, doi:10.1029/2002RS002750.

Antonov, J. I., S. Levitus, T. P. Boyer, M. E. Conkright, T. D. O'Brien, and C. Stephens, 1998: *World Ocean Atlas 1998. Vol. 4: Salinity of the Atlantic Ocean*. NOAA Atlas NESDIS 27, 166 pp.

Bentamy, A., P. Queffeulou, Y. Quilfen, and K. Katsaros, 1999: Ocean surface wind fields estimated from satellite active and passive microwave instruments. *IEEE Trans. Geosci. Remote Sens.,* **37,** 2469–2486.

Blume, H. J. C., A. W. Love, M. J. V. Melle, and W. W. Ho, 1977: Radiometric observations of sea temperature at 2.65 GHz over Chesapeake Bay. *IEEE Trans. Geosci. Remote Sens.,* **AP-25,** 121–128.

Bourassa, M. A., M. H. Freilich, D. Legler, W. T. Liu, and J. J. O. Brien, 1997: Wind observations from new satellite and research vessels agree. *Eos, Trans. Amer. Geophys. Union,* **78,** 597–602.

Boutin, J., and J. Etcheto, 1991: Intrinsic error in the air–sea CO_2 exchange coefficient resulting from the use of satellite wind speeds. *Tellus,* **43B,** 236–246.

Camps, A., and Coauthors, 2001: Wind and Salinity Experiment 2000 (WISE 2000). Scientific Analysis Report. ESTEC Contract 14188/00/NL/DC, 94 pp.

——, and Coauthors, 2002: Sea Surface Emissivity Observations at L-band: First results of the Wind and Salinity Experiment WISE-2000. *IEEE Trans. Geosci. Remote Sens.,* **40,** 2117–2130.

Dickinson, S., K. A. Kelly, M. J. Caruso, and M. J. McPhaden, 2001: Comparisons between the TAO buoy and NASA scatterometer wind vectors. *J. Atmos. Oceanic Technol.,* **18,** 799–806.

Dinnat, E., J. Boutin, G. Caudal, J. Etcheto, and P. Waldteufel, 2002: Influence of sea surface emissivity model parameters in L-band for the estimation of salinity. *Int. J. Remote Sens.,* **23,** 5117–5122.

——, ——, ——, ——, and A. Camps, 2003a: Issues concerning the sea emissivity modeling in L-band for retrieving surface salinity. *Radio Sci.,* **38,** 8060, doi:10.1029/2002RS002637.

——, ——, ——, ——, and S. Contardo, 2003b: On the use of EUROSTARRS and WISE data for validating L-band emissivity models. *Proc. First Results Workshop on EuroSTARRS, WISE, LOSAC Campaigns,* Toulouse, France, ESA SP-525, 117–124.

Dunbar, S., B. Weiss, S. Stiles, J. Huddleston, P. Callahan, G. Shirtliffe, K. Perry, and C. Hsu, 2001: QuikSCAT science data product user's manual. JPL Publ. D-18053, 95 pp.

Durden, S. L., and J. F. Vesecky, 1985: A physical radar cross-section model for a wind-driven sea with swell. *IEEE J. Oceanic Eng.* **OE-10,** 445–451.

Etcheto, J., E. P. Dinnat, S. Contardo, and J. Boutin, 2003: Comparison of EUROSTARRS and WISE measurements with sea surface emissivity models. *Proc. First Results Workshop on EuroSTARRS, WISE, LOSAC Campaigns,* Toulouse, France, ESA SP-525, 133–136.

——, ——, J. Boutin, A. Camps, J. Miller, S. Contardo, J. Wesson, J. Font, and D. Long, 2004: Wind speed effect on L-band brightness temperature inferred from EuroSTARRS and WISE 2001 field experiments. *IEEE Trans. Geosci. Remote Sens.,* in press.

Freilich, M. H., and R. S. Dunbar, 1999: The accuracy of NSCAT1 vector winds: Comparisons with National Data Buoy Center buoys. *J. Geophys. Res.,* **104,** 11 231–11 246.

Jackson, D. D., 1972: Interpretation of inaccurate, insufficient and inconsistent data. *Geophys. J. Roy. Astrophys. Soc.,* **28,** 97–109.

Kelly, K. A., S. Dickinson, M. J. McPhaden, and G. C. Johnson, 2001: Ocean currents evident in satellite wind data. *Geophys. Res. Lett.,* **28,** 2469–2472.

Kerr, Y., P. Waldteufel, J. P. Wigneron, J. M. Martinuzzi, J. Font, and M. Berger, 2001: Soil moisture retrieval from space: The soil moisture and ocean salinity mission (SMOS). *IEEE Trans. Geosci. Remote Sens.,* **39,** 1729–1735.

Klein, L. A., and C. T. Swift, 1977: An improved model for the dielectric constant of sea water at microwave frequencies. *IEEE Trans. Antennas Propag.,* **AP-25,** 104–111.

Lagerloef, G. S. E., C. F. Swift, and D. M. L. Vine, 1995: Sea surface salinity: The next remote sensing challenge. *Oceanography,* **8,** 44–50.

LeVine, D. M., and S. Abraham, 2002: The effect of the ionosphere on remote sensing of sea surface salinity from space: Absorption and emission at L-band. *IEEE Trans. Geosci. Remote Sens.,* **40,** 771–782.

Lewis, E., 1980: The practical salinity scale 1978 and its antecedents. *IEEE J. Oceanic Eng.,* **OE-5,** 3–8.

Marquardt, D. W., 1963: An algorithm for least-squares estimation of non-linear parameters. *J. Soc. Ind. Appl. Math,* **11,** 431–441.

Quilfen, Y., B. Chapron, and V. Vandemark, 2001: The ERS scatterometer wind measurement accuracy: Evidence of seasonal and regional biases. *J. Atmos. Oceanic Technol.,* **18,** 1684–1697.

Reul, N., and B. Chapron, 2002: Effects of foam on the emissivity of the sea surface at L-band (WP1300 report). Scientific requirements and impact of space observation of ocean salinity for modeling and climate studies. Final Rep. of ESA Contract 14273/00/NL/DC, 1–42.

Reynolds, R. W., and T. M. Smith, 1994: Improved global sea surface temperature analyses using optimum interpolation. *J. Climate,* **7,** 929–948.

Silvestrin, P., M. Berger, Y. H. Kerr, and J. Font, 2001: ESA's Second Earth Explorer Opportunity Mission: The Soil Moisture and Ocean Salinity Mission—SMOS. *IEEE Geosci. Remote Sens. Soc. Newsl.,* **118,** 11–14.

Skou, N., 2003: Faraday rotation and L-band oceanographic measurements. *Radio Sci.,* **38,** 8059, doi:10.1029/2002RS002671.

Swift, C. T., and R. E. McIntosh, 1983: Considerations for microwave remote sensing of ocean-surface salinity. *IEEE Trans. Geosci. Remote Sens.,* **GE21,** 480–490.

Waldteufel, P., and G. Caudal, 2002: Off-axis radiometric measurements: Application to interferometric antenna designs. *IEEE Trans. Geosci. Remote Sens.,* **40,** 1435–1439.

——, J. Boutin, and Y. Kerr, 2003: Selecting an optimal configuration for the SMOS mission. *Radio Sci.,* **38,** 8051, doi:10.1029/2002RS002744.

Yueh, S. H., 1997: Modeling of wind direction signals in polarimetric sea surface brightness temperatures. *IEEE Trans. Geosci. Remote Sens.,* **35,** 1400–1418.

——, R. West, W. J. Wilson, K. K. Li, E. G. Njoku, and Y. Rahmat-Samii, 2001: Error sources and feasibility for microwave remote sensing of ocean surface salinity. *IEEE Trans. Geosci. Remote Sens.,* **39,** 1049–1060.